Optimisation of Cu_2ZnSnS_4 solar cells with CuSCN as an inorganic hole-transport material

Muteeu A. Olopade[a,b],Soko Swaray[b], MuniruAmara[b]

[a]Department of Physics, University of Lagos, Nigeria

[b] Department of Physics, Fourah Bay College, University of Sierra Leone, Sierra Leone

ABSTRACT

Given the paucity of studies addressing realistic defect physics and the long-term stability of CZTS for photovoltaic use, this study seeks to enhance CZTS solar-cell performance via SCAPS-1D modelling. We examine how device parameters, layer thicknesses, operating temperature, defect concentrations, and capture cross-sections influence the solar cell metrics. The modelled device stack comprises 90 nm indium tin oxide (ITO) transparent conductor, 400 nm titanium dioxide (TiO2) as the electron transport layer (ETL), a 200 nm p-type Copper Zinc Tin Sulphide (CZTS) absorber, an 80 nm copper(I) thiocyanate (CuSCN) hole transport layer (HTL), and a metallic back contact. CZTS exhibits strong absorption in the visible range (>105 cm? ¹). Simulated J–V behaviour shows a short-circuit current density of - 18 mA/cm² and an open-circuit voltage of 0.7 V, while the external quantum efficiency (QE) in the UV–visible range exceeds 100% in places. Optimizing TiO2 ETL thickness in the 350–400 nm window achieves a PCE of 10.98%; CuSCN HTL thickness in the 20–40 nm range yields a peak of 11.32% (with near-identical performance from 20–85 nm). Balancing absorption with electronic quality led to an optimal absorber thickness near 300 nm, producing 13.34% efficiency. Peak device efficiency reached about 13.0% around 550 K, whereas increasing absorber defect concentration from 10^{13} to 10^{18} cm? ³ degraded absorber behaviour through Shockley–Read–Hall recombination. Extremely small defect capture cross-sections produced high efficiencies (22.3% and ~24%). These findings stress the importance of defect passivation and interface engineering for achieving competitive CZTS cell performance.

Key words

CZTS, Photovoltaic, Defect density, Capture cross-section, Operating temperature

* Corresponding author.

E-mail address: molopade@unilag.edu.ng

1. INTRODUCTION

Renewable power has become central to sustainable development goals. Historically, industries, transport, and modern lifestyles have relied heavily on fossil fuels such as coal, oil, and natural gas (Rocha-Meneses et al., 2023). This dependence has, however, led to serious environmental and societal problems climate change, air pollution, depletion of resources, and geopolitical tensions (KarlilarPata&Balcilar, 2024). By contrast, renewable sources solar, wind, hydro, biomass, and geothermal, generally offer cleaner, more sustainable, and often more cost-effective alternatives to traditional fossil fuels (Rossi & Bianchi, 2024). Deploying renewables reduces emissions, strengthens energy security, supports economic development, and benefits communities (Gan et al., 2023). Consequently, building sustainable energy systems that meet present needs while protecting the well-being of future generations is essential. These challenges raise critical concerns about safety and long-term reliability and motivate

research into safer, environmentally friendly energy options. Copper zinc tin sulphide (CZTS) is a promising kesterite absorber because of its earth-abundant composition, non-toxicity, bandgap in the 1.4–1.6 eV range, and strong absorption, making it suitable for low-cost thin-film photovoltaics (Dai et al., 2012). Nevertheless, achieving high device performance remains difficult. Although this study is driven by simulations and seeks to investigate theorical performance boundaries, the device parameters obtained have been compared with cutting edge experimental findings. The top efficiencies recorded for kesterite-based solar cells have reached 12.6% for CZTSSe devices(Kumar & Thakur, 2018). With more recent development indicating efficiencies nearing ~13% under optimal conditions(K.-J. Yang et al., 2019). In contrast, pure CZTS device generally achieve efficiencies between 9-11%, primarily constrained by high defect densities, band tailing, and non-radiative recombination losses(Xu et al., 2022). Numerical tools such as SCAPS-1D have been employed to explore and optimize device parameters (Buffière et al., 2015). From buffer-layer engineering to band alignment and interface recombination control, simulation studies aim to narrow the gap to theoretical efficiency limits (potentially above 30%). Some theoretical works project optimistic PCEs, for example, 24–26% by employing advanced back-surface-field materials and heterojunction designs (P. Srivastava et al., 2022). However, a sizable disparity persists between simulated predictions and experimental realizations. Recent reviews point out that SCAPS-1D studies can produce unrealistically high PCEs due to idealized assumptions about defects and recombination (Sherkar et al., 2017). Realistic defect physics and stability issues in kesterite make surpassing 20% PCE a formidable challenge and call for closer experimental validation of simulation results. This work addresses that need by optimizing ETL, HTL, and absorber thicknesses, operating temperature, defect densities, and electron/hole capture cross-sections based on experimentally relevant ranges.

1. METHODOLOGY

2.1 Device Structure and Design

Device Structure and Design: CZTS solar cells were simulated using SCAPS-1D, developed at Ghent University (Zyoud et al., 2021). The modelled stack included 90 nm Indium Tin Oxide (ITO) as a transparent conductor, 400 nm TiO_2 as ETL, 200 nm p-type CZTS absorber, and 80 nm CuSCN HTL with a metallic rear contact. Electronic parameters were taken from literature sources (Ghosh et al., 2022). Optically, the model emphasized absorption in the CZTS layer while treating ITO and TiO_2 as transparent. Simulations used the AM1.5G spectrum (1000 W/m²)

at 300 K, workfunction for both front and backcontacts are given as 4.5 eV and 5.2 Ev respectively,with an absorption coefficient of $10^5 cm^{-1}$ (Hafaifa et al., 2025),and extracted Voc, Jsc, FF, PCE, and QE curves. We probed how absorber thickness and defect densities affect performance and identified limiting loss mechanisms, employing TiO2 and CuSCN as non-toxic transport layers. Table 1 lists the baseline simulation parameters and Table 2 interface parameters. The simulator solves carrier dynamics via Poisson, continuity, and drift–diffusion equations. Relations for potential and space charge are given in Equations 1–4(Choudhury, 2025).

$$\frac{d^2\Psi(X)}{dX^2} = -\frac{dE(X)}{dX} = \frac{q}{\varepsilon}(n - p + N_A^- - N_D^+) \qquad (1)$$

Here, Ψ denotes the semiconductor electrostatic potential, E the electric field, q the elementary charge, and ε the permittivity. The equilibrium free-carrier concentrations are n and p at equilibrium with N_A^- and N_D^+. The continuity equations describing electron and hole behaviour in the absorber are shown by Equations (Hamammu, 2013).

$$\left(\frac{\delta p}{\delta t}\right)_{drift} + \left(\frac{\delta p}{\delta t}\right)_{diff} + \left(\frac{\delta p}{\delta t}\right)_{G} = 0 \qquad (2)$$

$$\left(\frac{\delta n}{\delta t}\right)_{drift} + \left(\frac{\delta n}{\delta t}\right)_{diff} + \left(\frac{\delta n}{\delta t}\right)_{G} = 0 \qquad (3)$$

In these expressions, p and n denote hole and electron densities, and G is the optical generation rate of photocarriers in the absorber. Diffusion length quantifies how far carriers travel in the absorber; according to Equation 5 it depends on the diffusion coefficient and carrier lifetime:

$$L = \sqrt{D\tau} \qquad (4)$$

L is the diffusion length and ?1s the carrier lifetime.

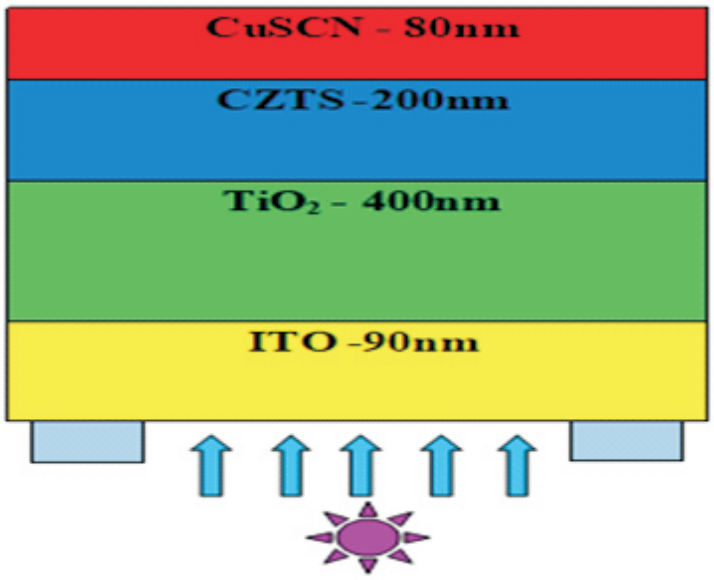


Figure 1 depicts a schematic of the CZTS solar cell.

Table 1: Initial Numerical Simulation Parameters

PARAMETERS	**CuSCN**	**CZTS**	**TiO_2**	**ITO**
Thickness (nm)	80	200	400	90
Bandgap (eV)	3.4	1.5	3.2	3.5
Electron affinity (eV)	1.9	4.5	3.9	4
Dielectric permittivity	10	10	9	9
CB effective density of states (cm^{-3})	2.2×10^{18}	2.2×10^{18}	1.0×10^{19}	2.2×10^{18}
VB effective density of states (cm^{-3})	1.8×10^{18}	1.8×10^{19}	1.0×10^{19}	1.8×10^{19}
Electron thermal velocity ($cm\ s^{-1}$)	1×10^{7}	1×10^{7}	1.0×10^{7}	1×10^{7}
Hole thermal velocity (cm^{-1})	1×10^{7}	1×10^{7}	1×10^{7}	1×10^{7}
Electron mobility (cm2/VJ)	100	100	20	20
Hole mobility (cm2/Vs)	25	25	10	10
Shallow uniform donor density, ND (cm^{-3})	0	1.0×10^{1}	1.0×10^{16}	1×10^{17}
Shallow uniform acceptor density, Nu (cm^{-3})	1.0×10^{20}	2.0×10^{14}	0	0
Defect type	-	Donor	-	-
Defect density (cm^{-3})	1.0×10^{15}	1×10^{13}	1×10^{11}	0
Reference	(Njema et al., 2024)	(Mazumder & Senthilkumar, 2022)	(Jhuma et al., 2019)	(Sravani et al., 2021)

Table 2: Energy level and interface parameters

Parameters	$CZTS/TiO_2$	CuSCN/ CZTS
Interface defect density	$10^{-12}\ cm^2$	$10^{-12}\ cm^2$
Trap energy level	Mid-gap	Mid-gap
Electron capture cross-section	$10^{-19}\ cm^2$	$10^{-19}\ cm^2$
Hole capture cross-section	$10^{-19}\ cm^2$	$10^{-19}\ cm^2$
Reference for defect energy level Et	Above the highest eV	Above the highest eV
Energy with respect to Reference (eV)	0.600	0.600
Energetic distribution	Single	Single

3 RESULTS AND DISCUSSION

3.1 Absorption coefficient of the CZTS solar cell

The absorption coefficient describes how efficiently a material absorbs photons across wavelengths. Absorption occurs when a photon's energy promotes an electron from the valence to the conduction band; the onset of strong absorption is set by the bandgap, summarized by $E=\frac{hc}{\lambda}$ (Chen et al., 2022). When photon energy exceeds the bandgap, absorption rises sharply, dropping off below the threshold. CZTS displays a marked increase in the visible region with absorption coefficients beyond 10^5 cm^{-1} (Zhang et al., 2016). a typical signature of a direct-bandgap semiconductor, where electronic transitions do not require phonon assistance. Consequently, CZTS can absorb strongly even in thin films (Nolan, 2012). Materials with larger bandgaps, such as CuSCN, remain largely transparent in the visible and contribute minimally to absorption while supporting hole transport. Sharp absorption edges indicate direct transitions; layers with bandgaps larger than visible wavelengths act as window layers, transmitting visible photons while providing conductivity. Photon-driven electronic transitions are illustrated in Figure 2.

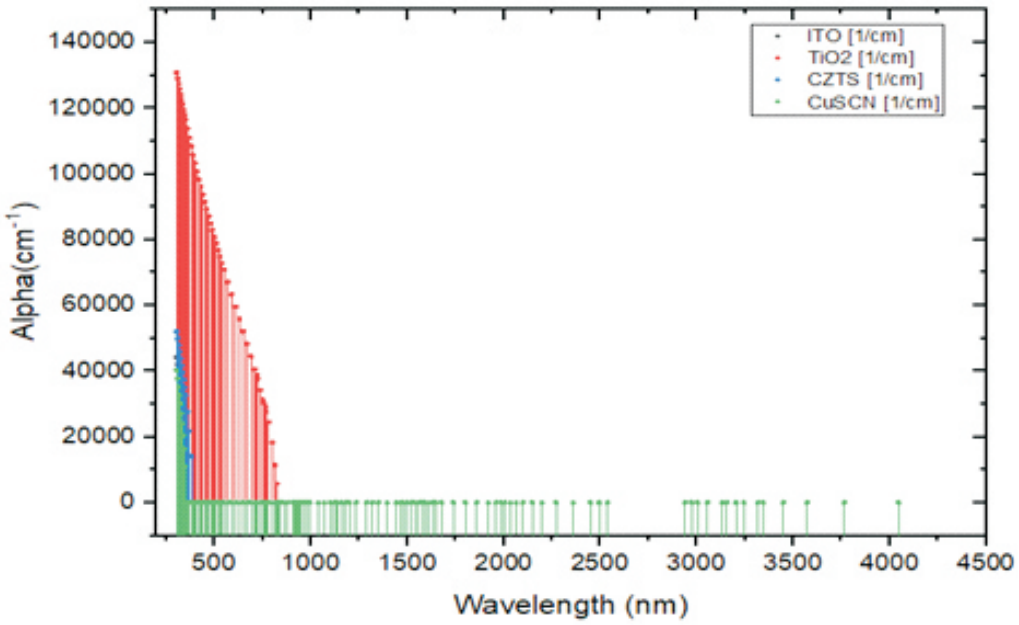


Figure 2: Absorption coefficient of ETL, CZTS absorber, and HTLs layers

3.2 J - V Curve for the CZTS Solar cell device

At low bias, the current density remains roughly constant at −18 mA/cm², representing the short-circuit current density (Jsc) when the cell's terminals are shorted, where the negative sign follows the SCAPS convention indicating current flowing out of the device, this corresponds to a magnitude of 18 mA/cm², which falls within the range reported for CZTS (Gordillo et al., 2019). Jsc reflects how effectively photons are absorbed and photogenerated carriers are collected. The built-in electric field of the p–n junction

separates photocarriers to produce photocurrent. As forward bias increases, the opposing field reduces net photocurrent; near V ≈ 0.7 V the net current approaches zero, marking the open-circuit voltage (Voc) where photocurrent balances diode dark current. Voc depends on the absorber's bandgap, recombination mechanisms, and temperature(Brus et al., 2021). The voltage–current region between Jsc and Voc contains the maximum power point (MPP), where power output is maximized by the current–voltage balance. The fill factor (FF) quantifies how square the J–V curve is and thus how effectively light is converted to electrical power. The curve shape indicates a moderate FF (Figure 3). PCE (η) is calculated as: $\eta = \frac{J_{mp} \cdot V_{mp}}{P_{in}}$ where Jmp and Vmp are the current density and voltage at MPP, and Pin is the incident

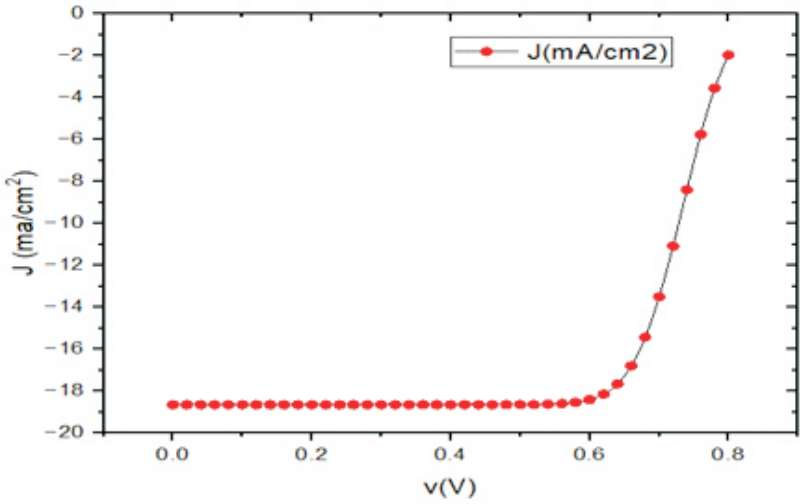


Figure 3: Characteristic J-V curve of CZTS device.

3.3 Energy Band Alignment of the CZTS Device

The step-like band gap profile was translated into a physically consistent band diagram by incorporating electron affinity -base band alignment. The front wide bandgap layer (Eg ≈ 3.4 Ev) forms a small positive conduction band offset with the CZTS absorber, which supress interface recombination while maintaining efficient electron transport. Within the absorber (Eg ≈ 1.5 Ev), band bending at the heterojunction facilitates efficient charge separation and enhances quasi-Femi level splitting, thereby contributing to the high open circuit voltage. At the interface, the wide band gap (Eg ≈ 3.2-3.5 eV) introduces a reflective barrier for minority carriers, reducing recombination losses. This energetically favorable E_c/E_v alignment ensures efficient carrier extraction and underpins the high simulated device performance.

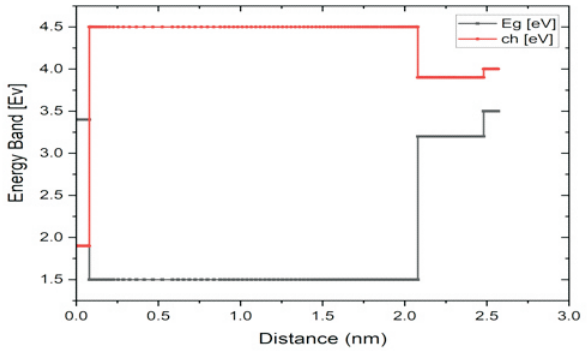


Figure 4: Energy band of the CZTS device.

3.4 Quantum efficiency characteristics

Quantum efficiency (QE) measures how many incident photons are converted into collected charge carriers (electrons and holes) and is a key indicator of spectral device performance (Matioli et al., 2011). Figure 5 presents the QE spectrum of the CZTS-based device. The detector exhibits strong photo response across the visible spectral region, with QE exceeding 80% between approximately 400 and 650 nm and reaching a maximum of 96% near 380 nm. The high QE at shorter wavelengths is attributed to the large optical absorption coefficient of CZTS, which enables efficient absorption of high-energy photons and rapid generation of electron hole pairs near the surface region where carrier collection is effective (Sahoo et al., 2021). The high peak QE indicates efficient photocarrier generation and minimal optical losses within the active layer. QE falls at longer wavelengths as photon energies approach the bandgap, reducing absorption and thus carrier generation, fewer photons are absorbed in the active layer when the absorption coefficient is lower at long wavelengths. QE approaches zero near ~820 nm which is consistence with the bandgap energy of CZTS (1.5 Ev) (Lotfy et al., 2025). Beyond this threshold, photons do not possess sufficient energy to generate electron-hole pairs, resulting in negligible photo response which is consistence with the intrinsic optical absorption characteristics of CZTS-base absorber materials.

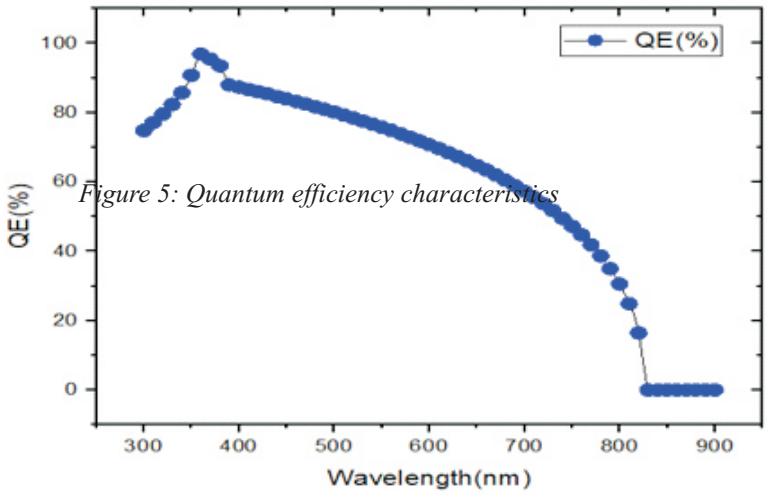


Figure 5: Quantum efficiency characteristics

Figure 5: Quantum efficiency characteristics

3.5 Impact of the variation of TiO_2 Electron Transport Layer thickness on device performance

Impact of the variation of TiO_2 Electron Transport Layer thickness on device performance. ETL thickness plays a critical role in the extraction of electrons and blocking of holes to limit recombination losses (Chu et al., 2019). ETLs that are too thin can leave pinholes or incomplete coverage, leading to shunts, elevated recombination, and degraded FF, Voc, and stability (Jeong et al., 2017). Conversely, overly thick ETLs increase series resistance and lengthen diffusion paths, impeding electron extraction and lowering Jsc and FF; excessive thickness can also introduce optical losses via absorption or scattering (Raj et al., 2025). Our simulations scanning TiO2 thicknesses from 350 to 1000 nm show a peak PCE of 10.98% at 350–400 nm, falling to 10.69% at 1000 nm due to poorer

charge extraction. FF decreased from 66.45% at 400 nm to 64.95% at 1000 nm. The Jsc peaked around 18.6892 mA/cm² for the 700–800 nm range while Voc varied only slightly (0.89718–0.89547 V). Overall, TiO2 thicknesses of approximately 500–700 nm provided the best trade-off between transport efficiency and recombination losses in our model (Figure 6).

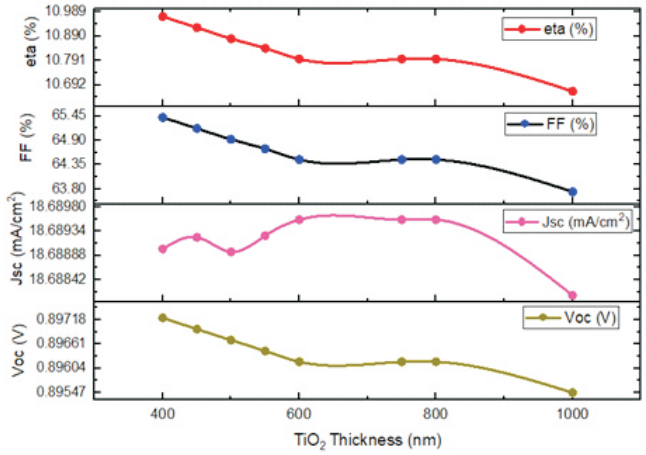


Figure 6: Electron Transport Layer (ETL) thickness vs. device metrics.

3.6 Impact of the variation of CuSCN Hole Transport Layer thickness on device performance

Impact of the variation of CuSCN Hole Transport Layer thickness on device performance. HTL thickness influences device efficiency by affecting surface coverage, hole extraction, series resistance, and interfacial quality (Riyad et al., 2023). We varied CuSCN thickness from 5 to 85 nm (Figure 7). Efficiency rose from 11.31540% at 5 nm to 11.31544% at 20–85 nm because very thin films suffer incomplete coverage and associated resistive losses, whereas thicker films beyond ~20 nm ensure continuous coverage, stabilizing charge transport and collection (Qasim et al., 2021). FF slightly decreased from 67.41% at 5 nm to 67.40% at 85 nm, reflecting increased series resistance for thicker HTLs. Jsc improved marginally from 18.66179 mA/cm² at 5 nm to 18.66187–18.66188 mA/cm² at 20–85 nm, and Voc rose from 0.8994651 V at 5 nm to 0.8994653–0.8994654 V at 30–85 nm, indicating better interfacial quality. We identify 20–40 nm as an optimal CuSCN thickness window, balancing efficiency, current, voltage, and minimal resistive loss: thinner layers risk incomplete coverage; thicker layers increase resistance without PCE gains.

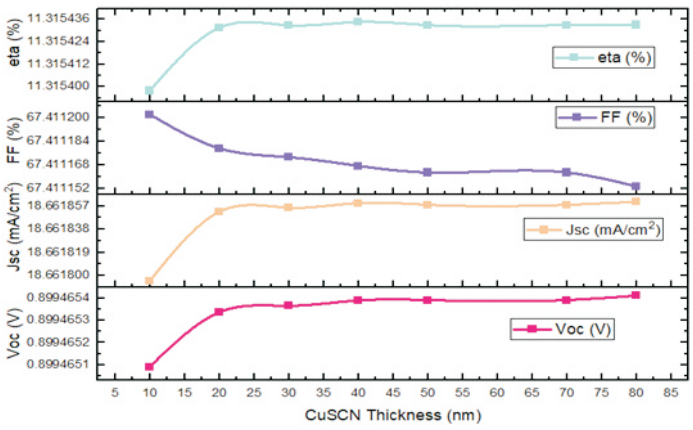


Figure 7: Hole Transport Layer (ETL) thickness vs. device metrics.

3.7 Impact of the variation of absorber thickness on device performance

The absorber layer is essential to the operation of a solar cell. Its thickness has a large bearing on a solar cell's efficiency as an electrical power generator (A. Srivastava et al., 2024). The absorber thickness strongly affects optical absorption, carrier generation/collection, recombination dynamics, and overall device performance (Cheragee&Alam, 2023). In CZTS, optimizing thickness balances light harvesting against electronic transport losses (Enayati Maklavani&Mohammadnejad, 2020a). Figure 8 shows that increasing absorber thickness from 265 nm to 300 nm raised Jsc slightly from 28.776 to 28.793 mA/cm², reflecting greater absorption. Reduced surface recombination led to Voc increasing from 0.73219 to 0.73295 V. FF moved from 63.30% to 63.276%, then to 63.28% at 300 nm, indicating transport losses were partially offset by improved collection. Efficiency varied such that η fell from 13.3397% at 265 nm to 13.3375% at 285 nm and rose to 13.3408% at 300 nm. Thus, 300 nm represents an optimal thickness in this model, balancing optical gains and electronic quality, a trend seen in other thin-film technologies where optical and transport trade-offs determine the best thickness (Bahador & Abdoli, 2024).The 200-300 nm CZTS absorber thickness, though thinner than conventional designs, is physically justified. CZTS's absorption coefficient exceeding $10^5 cm^{-1}$ allows 90% of visible photons to be absorbed within hundreds of nanometres, enabling efficient photogeneration(Cao et al., 2025). Reducing absorber thickness suppresses bulk recombination by shortening carrier transport distances, enhances field-assisted collection, and minimizes defects(Enayati Maklavani&Mohammadnejad, 2020b). Recent thin-film photovoltaic progress shows performance depends on absorption-recombination balance, with 200-300 nm representing an optimal range for high absorption and reduced losses(Li et al., 2021).

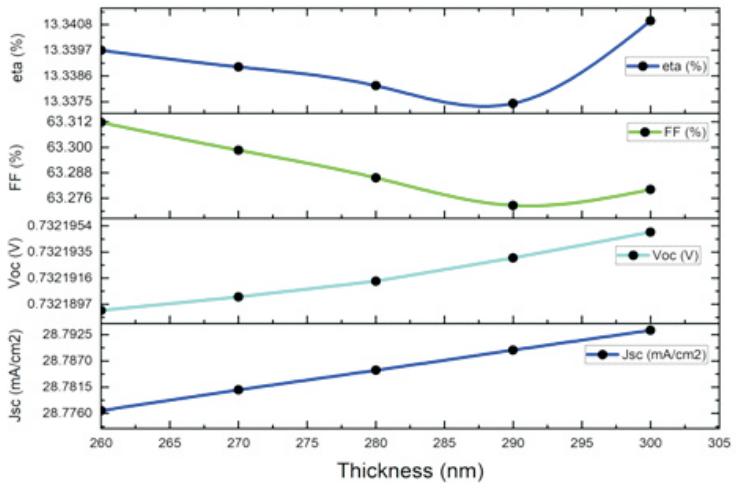


Figure 8: Absorber thickness in relation to important photovoltaic metrics

3.8 Effect of Working Temperature on Device Performance

Contour plots in Figure 9a–d illustrate temperature dependence of Voc, Jsc, FF, and η, shedding light on thermal effects and carrier dynamics. Voc initially increases with temperature and reaches a maximum (~1.10 V) near ~450 K, reflecting elevated carrier generation and enhanced built-in potential (Liu et al., 2018). Beyond ~600 K Voc falls below ~0.95 V as intrinsic carrier concentration and recombination increase, reducing quasi-Fermi level splitting photovoltage (Katz et al., 2001). Jsc declines modestly from ~18.652 mA/cm² as temperature rises, consistent with reduced carrier mobility and increased phonon scattering despite bandgap narrowing. FF shows a non-linear response dropping from ~72% at 300 K to ~60% near 450 K due to larger series resistance and recombination, with some recovery approaching 600 K as thermal energy aids charge extraction (reaching >65% of the initial value). Overall efficiency increases from ~11% to ~13% as the thermal energy increases from 300K to 500-600K. This behaviourarises from the exponential increase in saturation current in temperature, which leads toa decrease in Voc. However, the present result shows a slight improvement in the efficiency around 550K. This deviation from the conventional trend may be attributed to enhanced carrier transport and reduced trap-assisted recombination at moderate temperatures(Qi et al., 2024).The increase in thermalenergy can facilitate carrier release from localized defects states, thereby improving charge collection efficiency.Beyond this temperature this temperature range, the dominant effect of recombination and bandgap narrowinglead todecrease in device performance.

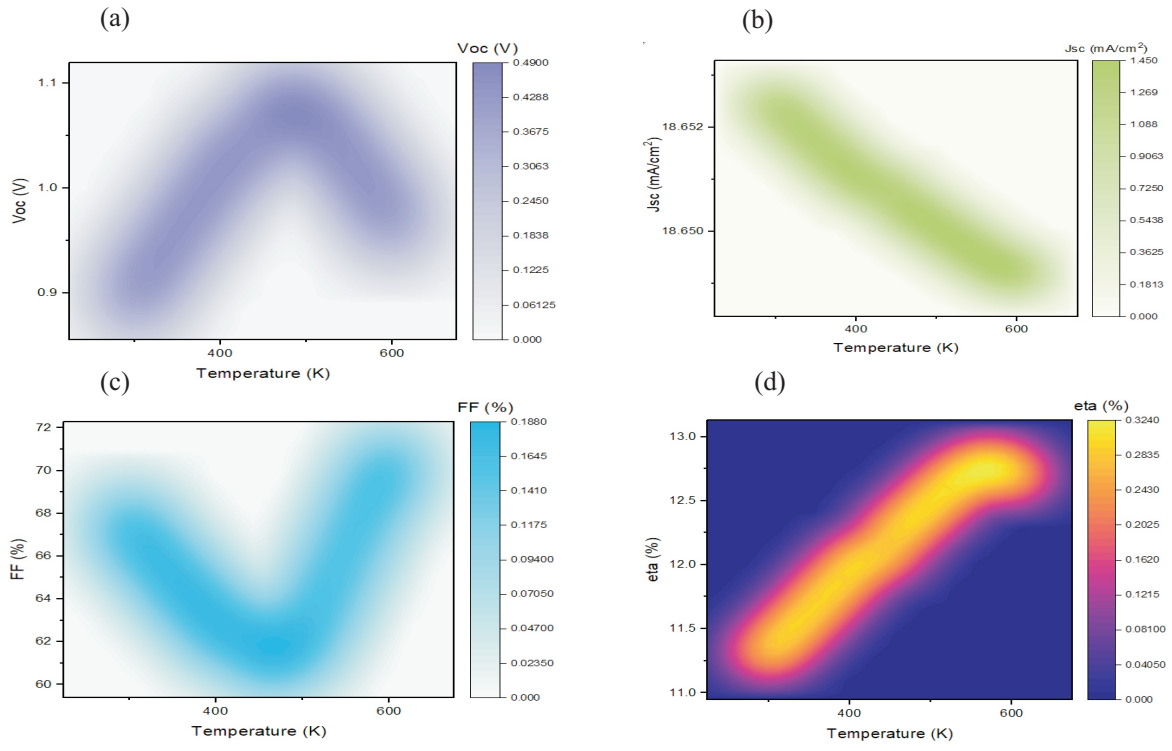


Figure 9a-d: Impact of Temperature on Photovoltaic Performance Parameters

3.9 Effect of CZTS absorber defect density on device performance

Localized defects in the absorber or at interfaces act as trap sites that mediate non-radiative Shockley–Read–Hall (SRH) recombination and degrade carrier dynamics(Das Adhikari et al., 2025). Increased trap density reduces Voc, Jsc, FF, and η, highlighting the need to minimize defect concentrations for efficient devices(Kavanagh et al., 2022). In SRH recombination, defects shorten carrier lifetimes and diffusion lengths, causing trap-assisted recombination to raise reverse saturation current and lower Voc(X. Yang et al., 2020). Enhanced recombination also diminishes Jsc and worsens diode idealist and resistive losses, lowering FF (Karki et al., 2019). Since η scales with Voc × Jsc × FF, defect density is a central factor limiting efficiency. For instance, with defect density 1×10^{14} cm^{-3},our modelled device yields Voc ≈ 1.40 V, Jsc ≈ 19.0 mA/cm², FF ≈ 78%, and η ≈ 18.0%. Increasing defects to 1×10^{19} cm^{-3} reduces Voc to ≈ 0.48 V, Jsc to ≈ 5.0 mA/cm², FF to ≈ 32%, and η to ≈ 1.5%, representing dramatic percentage declines (66% in Voc, 74% in Jsc, 59% in FF, and 92% in η). These changes stem from amplified SRH recombination, higher dark saturation current, and shorter carrier lifetimes/diffusion lengths (Perl et al., 2017). Figures 10a–d illustrate this behaviour.

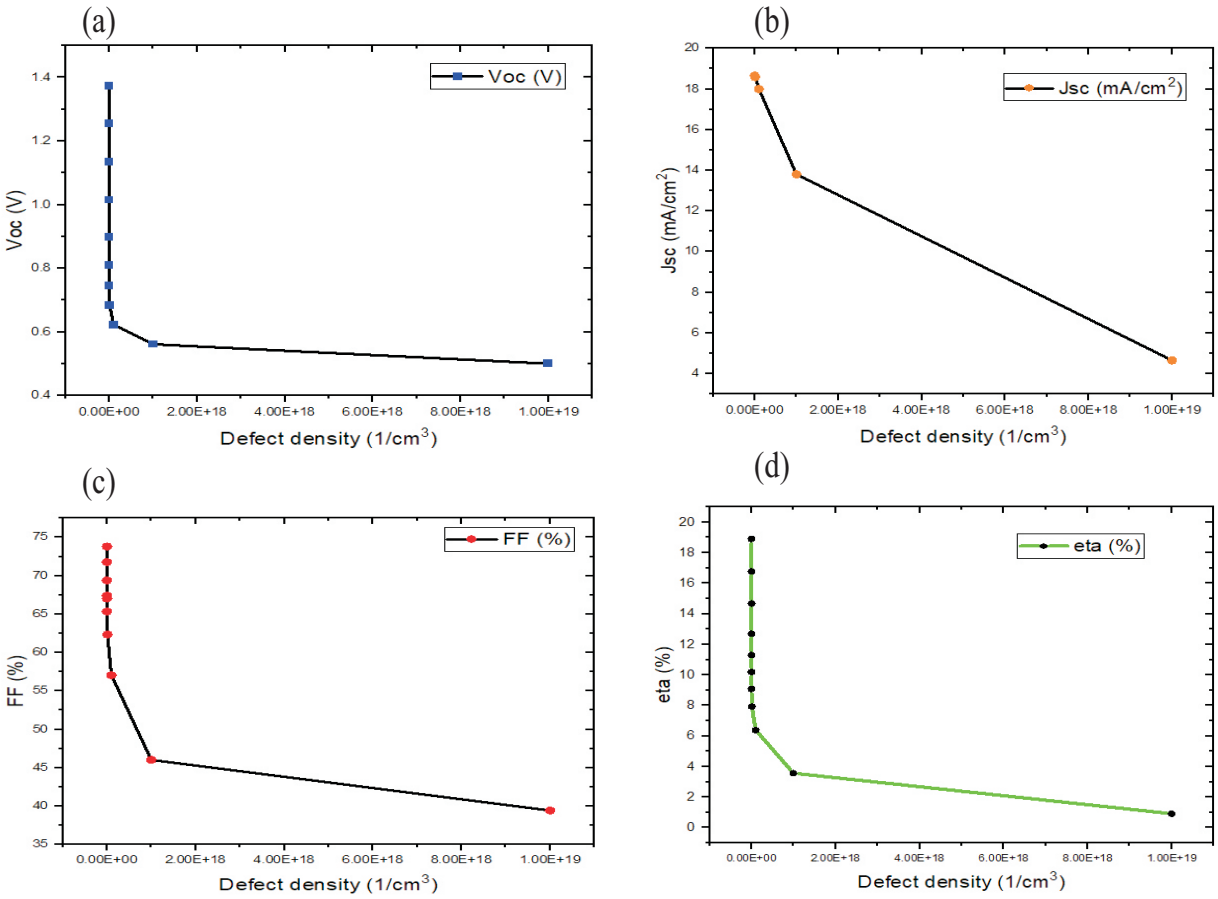


Figure 10a-d: Impact of absorber defect density on device performance.

3.10 Defect capture cross-section for electrons (σn) (cm²) on device performance

Device behaviour is strongly affected by both defect density Nt and the electron capture cross-section σn in the absorber (Yadav et al., 2024). Figures 11a–d present how Voc, Jsc, FF, and η vary with these parameters. As Nt increases in the n-type absorber, device performance degrades. For Nt = 1×10^{13} cm^{-3} the cell has Voc ˜ 0.61 V, Jsc ≈ 19.6 mA/cm², FF ˜ 74%, and η ˜ 22.3%. When Nt is raised to 1×10^{15} cm^{-3}, Voc falls to ~0.15 V, Jsc to ~13.8 mA/cm², FF to ~58%, and η drops below 2%. At Nt = 1×10^{18} cm^{-3} the device becomes essentially non-functional. These declines arise from increased SRH recombination: higher Nt provides more recombination centres and shortens carrier lifetimes(Tanaka & Kato, 2024). Concerning σn in the p-type absorber, very small σn values can produce non-physical outcomes in simulation; beyond σn = 10? ^{15} cm² Voc stabilizes near ~0.9 V with ~11% efficiency. Voc and η show strong dependence on σn while Jsc remain roughly constant (~18.65 mA/cm²). FF initially decreases but then improves with larger σn as carrier accumulation is mitigated. These results suggest Nt sets the overall recombination capacity while σn controls how effectively a defect centre recombines carriers. Since recombination rate U ? σ Nt, both parameters jointly determine carrier lifetime and efficiency losses (Kato et al., 2024). The high efficiency of 22.3% at Nt = 1×10^{13} cm^{-3} arises from suppress SHR recombination due to the reduced density of recombination-active centres and small capture cross -section, leading to enhance carrier lifetime, improved quasi-Femi level splitting, and near-diode behaviour(Leijtens et al., 2016). However, this condition represents an upper-limit scenario corresponding to near defect free absorber material(Kim et al., 2020).

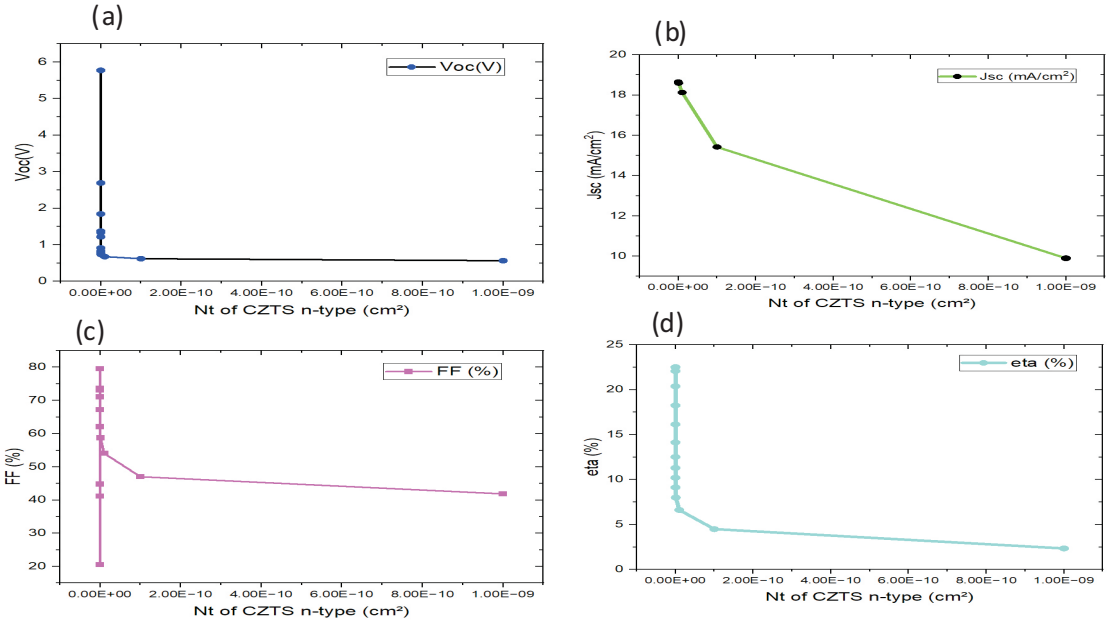


Figure 11a-d: illustrates the defect capture cross-section for electrons (σn).

3.11 Defect capture cross-section for holes (σp) (cm²) on device performance

Figures 12a–d show how the hole capture cross-section affects photovoltaic metrics. Capture cross-section has a strong impact on Voc and η, while Jsc and FF are comparatively insensitive. In simulations with negligible Nt, Voc can reach unrealistically large values (≈7.5 V), an artifact of idealized modelling. With realistic Nt values, Voc drops below 1.0 V due to SRH recombination (Maqsood et al., 2021) illustrating the pronounced Voc deficit characteristic of kesterite absorbers. Jsc remains nearly unchanged across Nt values (18.65246–18.65253 mA/cm²), implying photogeneration and collection are relatively unaffected by these recombination centres (He et al., 2021). Consequently, η increased to ~24% even when Jsc and FF remain stable, indicating Voc degradation is the dominant loss. The 24% efficiency observed at a hole capture cross-section arises from the strong suspension of hole-mediated Shockley-read-hall recombination in the absorber. At such low defect density and small σ_p, trap assisted recombination is minimized, leading to prolong minority carrier lifetime and efficient charge collection, which stabilizes Jsc and FF. The remaining efficiency is therefore governed primarily by changes in

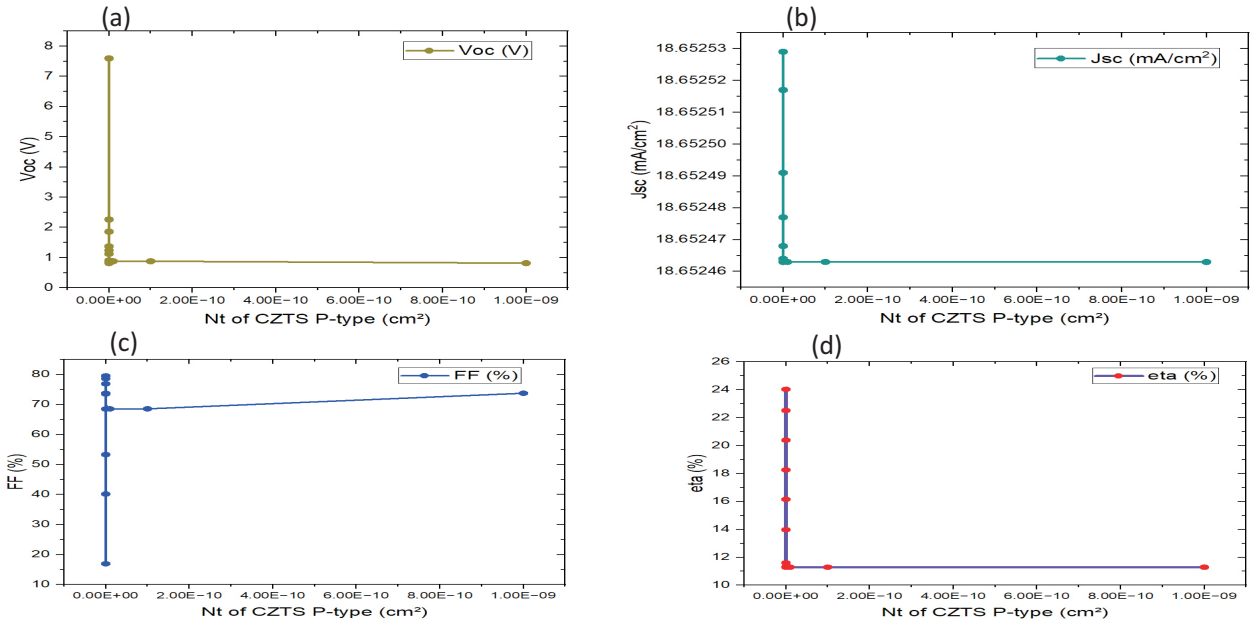


Figure 12a-d: Defect capture cross-section for holes (σp)

Conclusion

CZTS shows absorption of visible light, with coefficients exceeding 10 cm^{-1}, in line with direct bandgap semiconductors. TiO_2 and CuSCN were shown to be transparent to visible light and effective at window-based stacking, since these materials have large band gaps. The short-circuit current density (Jsc) of -18 mA/cm^2 and open circuit voltage (Voc) of 0.7 V were measured by the device, while the QE reaching a maximum of 96% near 380 nm. An optimum power conversion efficiency (PCE) of 10.98% was obtained with a TiO_2 thickness of 350–400 nm. A hole transport layer thickness (HTL) of 20–40 nm was found to produce an efficiency of 11.31544%. An absorber thickness of 300 nm balanced light and carrier taking for 13.3408%. This behaviour arises from the exponential increase in saturation current in temperature, which leads to a decrease in Voc. Increasing the defect density in CZTS to 10^{18} cm^{-3} decreases efficiency by 92% by SRH (Shockley-Read-Hall) recombination. Voc is affected by electron ($\sigma\ n$) and hole ($\sigma\ p$) capture cross-sections. Simulations indicate efficiencies of 22–24% could be attained with few defects. Optimized layer thickness, temperature control, and low defect density are necessary for CZTS cells to attain high efficiency.

References

Bahador, H., & Abdoli, Z. (2024). Enhancing light absorption in ultra-thin perovskite solar cells using plasmonic gold nanoparticle clusters. *Physica Scripta*, *99*(10), 105918. https://doi.org/10.1088/1402-4896/ad7074

Brus, V. V., Schopp, N., Ko, S., Vollbrecht, J., Lee, J., Karki, A., Bazan, G. C., & Nguyen, T. (2021). Temperature and Light Modulated Open- Circuit Voltage in Nonfullerene Organic Solar Cells with Different Effective Bandgaps. *Advanced Energy Materials*, *11*(4), 2003091. https://doi.org/10.1002/aenm.202003091

Buffière, M., Harel, S., Guillot-Deudon, C., Arzel, L., Barreau, N., & Kessler, J. (2015). Effect of the chemical composition of co-sputtered Zn(O,S) buffer layers on Cu(In,Ga)Se_2 solar cell performance: Chemical composition of co-sputtered Zn(O,S) buffer layers. *Physica Status Solidi (a)*, *212*(2), 282–290. https://doi.org/10.1002/pssa.201431388

Cao, Z., Liu, C., Li, J., Dong, J., Hu, S., Wang, W., Wu, X., & Zhang, Y. (2025). Thickness- dependent carriers transport in Sb_2 Se_3 thin film solar cells. *Rare Metals*, *44*(5), 3051–3059. https://doi.org/10.1007/s12598-024-03171-0

Chen, D., Shivarudraiah, S. B., Geng, P., Ng, M., Li, C.-H. A., Tewari, N., Zou, X., Wong, K. S., Guo, L., & Halpert, J. E. (2022). Solution-Processed, Inverted $AgBiS_2$ Nanocrystal Solar Cells. *ACS Applied Materials & Interfaces*, *14*(1), 1634–1642. https://doi.org/10.1021/acsami.1c17133

Cheragee, S. H., & Alam, M. J. (2023). Device modeling and numerical study of a double absorber solar cell using a variety of electron transport materials. *Heliyon*, *9*(7), e18265. https://doi.org/10.1016/j.heliyon.2023.e18265

Choudhury, A. N. R. (2025). EQUATIONS OF A SOLAR CELL. *International Journal of Engineering Science Technologies*, *9*(2). https://doi.org/10.29121/ijoest.v9.i2.2025.675

Chu, W., Li, X., Li, S., Hou, J., Jiang, Q., & Yang, J. (2019). High-Performance Flexible Perovskite Solar Cells with a Metal Sulfide Electron Transport Layer of SnS_2 by Room-Temperature Vacuum Deposition. *ACS Applied Energy Materials*, *2*(1), 382–388. https://doi.org/10.1021/acsaem.8b01405

Dai, P., Zhang, G., Chen, Y., Jiang, H., Feng, Z., Lin, Z., & Zhan, J. (2012). Porous copper zinc tin sulfide thin film as photocathode for double junction photoelectrochemical solar cells. *Chemical Communications*, *48*(24), 3006. https://doi.org/10.1039/c2cc17652a

Das Adhikari, R., Patel, M. J., Baishya, H., Yadav, D., Kalita, M., Alam, M., & Iyer, P. K. (2025). Decoding recombination dynamics in perovskite solar cells: An in-depth critical review. *Chemical Society Reviews*, *54*(8), 3962–4034. https://doi.org/10.1039/D4CS01231C

Enayati Maklavani, S., & Mohammadnejad, S. (2020a). The impact of the carrier concentration and recombination current on the p+pn CZTS thin film solar cells. *Optical and Quantum Electronics*, *52*(6), 279. https://doi.org/10.1007/s11082-020-02407-4

Enayati Maklavani, S., & Mohammadnejad, S. (2020b). The impact of the carrier concentration and recombination current on the p+pn CZTS thin film solar cells. *Optical and Quantum Electronics*, *52*(6), 279. https://doi.org/10.1007/s11082-020-02407-4

Gan, K. E., Taikan, O., Gan, T. Y., Weis, T., Yamazaki, D., & Schüttrumpf, H. (2023). Enhancing Renewable Energy Systems, Contributing to Sustainable Development Goals of United Nation and Building Resilience Against Climate Change Impacts. *Energy Technology*, *11*(11), 2300275. https://doi.org/10.1002/ente.202300275

Ghosh, S., Yasmin, S., Ferdous, J., & Saha, B. B. (2022). Numerical Analysis of a CZTS Solar Cell with MoS2 as a Buffer Layer and Graphene as a Transparent Conducting Oxide Layer for Enhanced Cell Performance. *Micromachines*, *13*(8), 1249. https://doi.org/10.3390/mi13081249

Gordillo, G., Calderón, C., & Moreno, R. (2019). Fabrication of solar cells based on Cu2ZnSnS4 films grown with optimized chemical composition homogeneity. *Revista de La Academia Colombiana de Ciencias Exactas, Físicas y Naturales*, *43*(166), 17. https://doi.org/10.18257/raccefyn.783

Hafaifa, L., Maache, M., Arteev, D., Rabhi, S., Djalab, Y., Bourhefir, R., Boudiar, M., Hafaifa, A., Adjouz, R., & Bouguenina, K. (2025). Optimization of CZTS absorber layer for enhanced efficiency in CZTS/CIGS tandem solar cells: A comprehensive loss analysis. *Physica Scripta*, *100*(9), 095530. https://doi.org/10.1088/1402-4896/ae00fd

Hamammu, I. M. (2013). *2 PUBLICATIONS 3 CITATIONS SEE PROFILE*.

He, M., Huang, J., Li, J., Jang, J. S., Suryawanshi, U. P., Yan, C., Sun, K., Cong, J., Zhang, Y., Kampwerth, H., Suryawanshi, M. P., Kim, J., Green, M. A., & Hao, X. (2021). Systematic Efficiency Improvement for $Cu_2ZnSn(S,Se)_4$ Solar Cells By Double Cation Incorporation with Cd and Ge. *Advanced Functional Materials*, *31*(40), 2104528. https://doi.org/10.1002/adfm.202104528

Jeong, I., Park, Y. H., Bae, S., Park, M., Jeong, H., Lee, P., & Ko, M. J. (2017). Solution-Processed Ultrathin TiO_2 Compact Layer Hybridized with Mesoporous TiO_2 for High-Performance Perovskite Solar Cells. *ACS Applied Materials & Interfaces*, *9*(42), 36865–36874. https://doi.org/10.1021/acsami.7b11901

Jhuma, F. A., Shaily, M. Z., & Rashid, M. J. (2019). Towards high-efficiency CZTS solar cell through buffer layer optimization. *Materials for Renewable and Sustainable Energy*, *8*(1), 6. https://doi.org/10.1007/s40243-019-0144-1

Karki, S., Marsillac, S., Paul, P., Rajan, G., Belfore, B., Poudel, D., Rockett, A., Danilov, E., Castellano, F., & Arehart, A. (2019). Analysis of Recombination Mechanisms in RbF-Treated CIGS Solar Cells. *IEEE Journal of Photovoltaics*, *9*(1), 313–318. https://doi.org/10.1109/JPHOTOV.2018.2877596

Karlilar Pata, S., & Balcilar, M. (2024). Decarbonizing energy: Evaluating fossil fuel displacement by renewables in OECD countries. *Environmental Science and Pollution Research*, *31*(21), 31304–31313. https://doi.org/10.1007/s11356-024-33324-8

Kato, M., Ogawa, A., Han, L., & Kato, T. (2024). Surface recombination velocities for 4H–SiC: Dependence of excited carrier concentration and surface passivation. *Materials Science in Semiconductor Processing*, *170*, 107980. https://doi.org/10.1016/j.mssp.2023.107980

Katz, E. A., Faiman, D., Tuladhar, S. M., Kroon, J. M., Wienk, M. M., Fromherz, T., Padinger, F., Brabec, C. J., & Sariciftci, N. S. (2001). Temperature dependence for the photovoltaic device parameters of polymer-fullerene solar cells under operating conditions. *Journal of Applied Physics*, *90*(10), 5343–5350. https://doi.org/10.1063/1.1412270

Kavanagh, S. R., Scanlon, D. O., Walsh, A., & Freysoldt, C. (2022). Impact of metastable defect structures on carrier recombination in solar cells. *Faraday Discussions*, *239*, 339–356. https://doi.org/10.1039/D2FD00043A

Kim, S., Márquez, J. A., Unold, T., & Walsh, A. (2020). Upper limit to the photovoltaic efficiency of imperfect crystals from first principles. *Energy & Environmental Science*, *13*(5), 1481–1491. https://doi.org/10.1039/D0EE00291G

Kumar, A., & Thakur, A. D. (2018). Improvement of efficiency in CZTSSe solar cell by using back surface field. *IOP Conference Series: Materials Science and Engineering*, *360*, 012027. https://doi.org/10.1088/1757-899X/360/1/012027

Le, T. T., Zhou, Z., Chen, A., Yang, Z., Rougieux, F., Macdonald, D., & Liu, A. (2024). Reassessing iron–gallium recombination activity in silicon. *Journal of Applied Physics*, *135*(13), 133107. https://doi.org/10.1063/5.0198737

Leijtens, T., Eperon, G. E., Barker, A. J., Grancini, G., Zhang, W., Ball, J. M., Kandada, A. R. S., Snaith, H. J., & Petrozza, A. (2016). Carrier trapping and recombination: The role of defect physics in enhancing the open circuit voltage of metal halide perovskite solar cells. *Energy & Environmental Science*, *9*(11), 3472–3481. https://doi.org/10.1039/C6EE01729K

Li, H., Hu, Y., Wang, H., Tao, Q., Zhu, Y., & Yang, Y. (2021). Full- Spectrum Absorption Enhancement in a- Si:H Thin- Film Solar Cell with a Composite Light- Trapping Structure. *Solar RRL*, *5*(3), 2000524. https://doi.org/10.1002/solr.202000524

Liu, G., Zhou, C., Wan, F., Li, K., Yuan, Y., Gao, Y., Lu, Y., & Yang, B. (2018). Dependence of power conversion properties of perovskite solar cells on operating temperature. *Applied Physics Letters*, *113*(11), 113501. https://doi.org/10.1063/1.5041028

Lotfy, L. A., Abdelfatah, M., Sharshir, S. W., El-Naggar, A. A., Ismail, W., & El-Shaer, A. (2025). Numerical simulation and optimization of FTO/TiO2/CZTS/CuO/Au solar cell using SCAPS-1D. *Scientific Reports*, *15*(1), 28022. https://doi.org/10.1038/s41598-025-12999-0

Maqsood, A., Li, Y., Meng, J., Qin, Z., Song, D., Qiao, B., Zhao, S., & Xu, Z. (2021). Organic Halide PEACl for Surface Passivation and Defects Suppression in Perovskite Solar Cells. *ACS Applied Energy Materials*, *4*(11), 12411–12420. https://doi.org/10.1021/acsaem.1c02210

Matioli, E., Neufeld, C., Iza, M., Cruz, S. C., Al-Heji, A. A., Chen, X., Farrell, R. M., Keller, S., DenBaars, S., Mishra, U., Nakamura, S., Speck, J., & Weisbuch, C. (2011). High internal and external quantum efficiency InGaN/GaN solar cells. *Applied Physics Letters*, *98*(2), 021102. https://doi.org/10.1063/1.3540501

Mazumder, S., & Senthilkumar, K. (2022). Device study and optimisation of CZTS/ZnS based solar cell with CuI hole transport layer for different conduction band offset. *Solar Energy*, *237*, 414–431. https://doi.org/10.1016/j.solener.2022.03.036

Njema, G. G., Kibet, J. K., Rono, N., & Meyer, E. L. (2024). Numerical simulation of a highly efficient perovskite solar cell based on $FeSi_2$ photoactive layer. *Nano Select*, *5*(9), 2400020. https://doi.org/10.1002/nano.202400020

Nolan, M. (2012). First-Principles Prediction of New Photocatalyst Materials with Visible-Light Absorption and Improved Charge Separation: Surface Modification of Rutile TiO_2 with Nanoclusters of MgO and Ga_2O_3. *ACS Applied Materials & Interfaces*, *4*(11), 5863–5871. https://doi.org/10.1021/am301516c

Qasim, I., Ahmad, O., Rashid, A., Zehra, T., Malik, M. I., Rashid, M., Ahmed, M. W., & Nasir, M. F. (2021). Numerical optimization of (FTO/ZnO/CdS/CH3NH3SnI3/GaAs/Au) perovskite solar cell using solar capacitance simulator with efficiency above 23% predicted. *Optical and Quantum Electronics*, *53*(12), 713. https://doi.org/10.1007/s11082-021-03361-5

Qi, S., Ge, C., Wang, P., Wu, B., Zhao, Y., Zhao, R., Shafian, S., Hua, Y., & Xie, L. (2024). Improving Perovskite Solar Cell Performance and Stability via Thermal Imprinting-Assisted Ion Exchange Passivation. *ACS Applied Materials & Interfaces*, *16*(38), 51037–51045. https://doi.org/10.1021/acsami.4c08538

Raj, M., Raj, A., Kishor, A., Kushwaha, A., & Goel, N. (2025). Advanced Computational Study on 144 Combinations of ETL & HTL Layers for High- Performance Cs2 TeI6 Solar Cells. *Advanced Theory and Simulations*, *8*(8), 2500341. https://doi.org/10.1002/adts.202500341

Riyad, Md. N. H., Sunny, A., Khatun, Most. M., Rahman, S., & Ahmed, S. R. A. (2023). Performance evaluation of WS_2 as buffer and Sb_2S_3 as hole transport layer in CZTS solar cell by numerical simulation. *Engineering Reports*, *5*(5), e12600. https://doi.org/10.1002/eng2.12600

Rocha-Meneses, L., Luna-delRisco, M., González, C. A., Moncada, S. V., Moreno, A., Sierra-Del Rio, J., & Castillo-Meza, L. E. (2023). An Overview of the Socio-Economic, Technological, and Environmental Opportunities and Challenges for Renewable Energy Generation from Residual Biomass: A Case Study of Biogas Production in Colombia. *Energies*, *16*(16), 5901. https://doi.org/10.3390/en16165901

Rossi, L., & Bianchi, G. (2024). Sustainable Solutions: Integrating Renewable Energy and Electric Vehicles for Cleaner Operations. *Journal of Energy Research and Reviews*, *16*(3), 52–63. https://doi.org/10.9734/jenrr/2024/v16i3342

Sahoo, G. S., Routray, S., Pradhan, K. P., & Mishra, G. P. (2021). Electrical, Optical, and Reliability Analysis of QD-Embedded Kesterite Solar Cell. *IEEE Transactions on Electron Devices*, *68*(11), 5518–5524. https://doi.org/10.1109/TED.2021.3076034

Sravani, L., Routray, S., Pradhan, K. P., & Piedrahita, M. C. (2021). Kesterite Thin- Film Solar Cell: Role of Grain Boundaries and Defects in Copper–Zinc–Tin–Sulfide and Copper–Zinc–Tin–Selenide. *Physica Status Solidi (a)*, *218*(16), 2100039. https://doi.org/10.1002/pssa.202100039

Srivastava, A., Ullas, A. V., & Roy, N. (2024). Efficiency enhancement and optimization of lead-free Cs_2PtI_6 perovskite solar cell. *Physica Scripta*, *99*(9), 095537. https://doi.org/10.1088/1402-4896/ad6d1c

Srivastava, P., Sadanand, Rai, S., Lohia, P., Dwivedi, D. K., Qasem, H., Umar, A., Akbar, S., Algadi, H., & Baskoutas, S. (2022). Theoretical study of perovskite solar cell for enhancement of device performance using SCAPS-1D. *Physica Scripta*, *97*(12), 125004. https://doi.org/10.1088/1402-4896/ac9dc5

Tanaka, K., & Kato, M. (2024). Carrier recombination in highly Al doped 4H-SiC: Dependence on the injection conditions. *Japanese Journal of Applied Physics*, *63*(1), 011002. https://doi.org/10.35848/1347-4065/ad160c

Wu, C., Wang, K., Yan, Y., Yang, D., Jiang, Y., Chi, B., Liu, J., Esker, A. R., Rowe, J., Morris, A. J., Sanghadasa, M., & Priya, S. (2019). Fullerene Polymer Complex Inducing Dipole Electric Field for Stable Perovskite Solar Cells. *Advanced Functional Materials*, *29*(12), 1804419. https://doi.org/10.1002/adfm.201804419

Xu, B., Qin, X., Lin, J., Chen, J., Tong, H., Qi, R., Yue, F., Chen, Y., Yang, P., Chu, J., & Sun, L. (2022). Positive Role of Inhibiting CZTSSe Decomposition on Intrinsic Defects and Interface Recombination of 12.03% Efficient Kesterite Solar Cells. *Solar RRL*, *6*(8), 2200256. https://doi.org/10.1002/solr.202200256

Yadav, A., Patel, A. K., & Mishra, R. (2024). Modelling and Simulation of CZTS Solar Cell using Zn_{1-x} Mg_x O as a buffer layer and Cul as a hole transport layer for efficiency improvement. *Engineering Research Express*, *6*(1), 015031. https://doi.org/10.1088/2631-8695/ad1849

Yang, K.-J., Kim, S., Kim, S.-Y., Ahn, K., Son, D.-H., Kim, S.-H., Lee, S.-J., Kim, Y.-I., Park, S.-N., Sung, S.-J., Kim, D.-H., Enkhbat, T., Kim, J., Jeon, C.-W., & Kang, J.-K. (2019). Flexible Cu2ZnSn(S,Se)4 solar cells with over 10% efficiency and methods of enlarging the cell area. *Nature Communications*, *10*(1), 2959. https://doi.org/10.1038/s41467-019-10890-x

Yang, X., Fu, Y., Su, R., Zheng, Y., Zhang, Y., Yang, W., Yu, M., Chen, P., Wang, Y., Wu, J., Luo, D., Tu, Y., Zhao, L., Gong, Q., & Zhu, R. (2020). Superior Carrier Lifetimes Exceeding 6 µs in Polycrystalline Halide Perovskites. *Advanced Materials*, *32*(39), 2002585. https://doi.org/10.1002/adma.202002585